Supplementary Information

A Novel Metal-Organic Framework Derived Carbon Nanoflower with Effective Electromagnetic Microwave Absorption and High-performance Electrochemical Energy Storage Properties

Liwei Zhu, [a,b#] Ning Liu, [a,#] Xincheng Lv, [a] Ziqiu Zhang, [a] Liangmin Yu, [a] Xia Li [a*]

[a] Key Laboratory of Marine Chemistry Theory and Technology, Ministry of Education; College of Chemistry and Chemical Engineering, Ocean University of China, Qingdao 266100, P.R China

[b] College of Chemistry and Chemical Engineering, Qilu Normal University, Shandong 266100, P.R, China

Experimental section

Materials and instruments

All reagents were commercially available and used without any further purification. Elemental analyses (C, H and N) were performed on a PerkinElmer 2400 Series II analyzer. Fourier transform infrared (FT-IR) spectra were recorded as KBr pellets on a Bruker Equinox 55 IR spectrometer in the range 4000−400 cm^{-1}. Thermogravimetric (TG) analyses were carried out using a NETZSCH STA 409 CD analyser with a heating rate of 10 °C·min^{-1} to 700 °C under a O_2 atmosphere. Powder X-ray diffraction (PXRD) patterns were collected on a Bruker D8 Avance X-ray powder diffractometer at 5 °C·min^{-1} sweep rate. The purity was determined by comparison of the simulated and experimental PXRD patterns. Topological analysis was performed and confirmed by the Topos program and the Systre software. The microwave assisted synthesis was performed in the CEM discovery microwave reactor.

Microwave-assisted synthesis of MOF 1

The synthesis of the flower-like is in a typical method: a mixture of $Cd(NO_3)_2{\cdot}4H_2O$ (0.03 g, 0.1 mmol) and Maleic hydrazide (MH, 0.034 g, 0.3 mmol) was dissolved in a mixture solution (DMF: ethanol=1:1, 10 mL) and placed in a 30 mL microwaves-transparent vial, which was heated to110 °C subsequently, and kept for 20 min under 100 W of microwave power. After natural cooling to room temperature, the precipitates were isolated by filtration, washing with mixture solution (DMF: ethanol=1:1) several times, to remove the unreacted raw materials, respectively.

Synthesis of MOF 2

A mixture of $Cd(NO_3)_2{\cdot}4H_2O$ (0.062 g, 0.2 mmol) and MH (0.067 g, 0.6 mmol) was dissolved in a mixture solution (DMF: ethanol=1:1, 6 mL). The mixture was heated at 120 °C for 72 h under autogenous pressure in a sealed 25 mL Teflon-lined stainless steel vessel then cooled to room temperature at a rate of 2 °C. h^{-1}. Yellow needle-like crystals of MOF were obtained by filtration, washing with DMF and acetone three times respectively and drying in air. Yiel of 47% (based on Cd). Anal. Calcd for $C_4H_2N_2O_2Cd$

(**1**): C 21.57, H 1, N 12.6%. Found: C 21.77, H 0.9, N 13.0. FT-IR (KBr pellets, cm^{-1}): 3385 (s), 1532 (w), 1499 (s), 1460(m), 1430 (vs), 1301 (s),1111(s), 867 (s).

Electrochemical measurement

Preparation of electrode materials

The flower complex was preoxidized at 250 °C for 2 h. The samples were carbonized at 500, 600 and 700 °C for 1h with a heating rate of 2 °C min^{-1} under N_2 atmosphere, named Cd-MOFs-500, Cd-MOFs-600 and Cd-MOFs-700, respectively.

For the working electrode, the active materials and polytetrafluoroethylene binder were mixed with a mass ratio of 9:1, and then pressed between two pieces of 1×1cm^2 nickel foam with a loading capacity of about 3 mg. Cyclic voltammetry (CV), electrochemical impedance spectroscopy (EIS) and galvanostatic charge-discharge (GCD) curves were collected from an Autolab electrochemical working station in a three-electrode system that assembled from a platinum sheet counter electrode, an Hg/HgO reference electrode and a working electrode under 2 M KOH electrolyte system. The cyclic voltammograms were acquired in a potential range between 0 and 0.5 V at different scan rates, and the charge-discharge processes were performed by cycling the potential from 0 to 0.3 V at different current densities. EIS was performed in a frequency range of 0.01 Hz to 100 KHz with a 5 mV amplitude at the open-circuit potential. The specific capacitance was calculated according to the following charge/discharge curves formula:

$$C = \frac{I\Delta t}{\Delta V m}$$

Where C is the specific capacitance (F g-1), I is charge/discharge current (A), Δ t is discharge time (s), m is the mass of active electrode materials (g), and ΔV is voltage window (V).

The measurement of EMWA

The details of dielectric measurement are added to "supporting information": the permeability and permittivity of the tested materials are measured on an Agilent E8363B vector network analyzer in the frequency range of 2–18 GHz. The mixture of 20 wt% of a powder absorber (the complexes) and paraffin in a 1: 4 wt ratio at 90 °C is uniformly mixed and is pressed into ring-shaped specimens (Φ_{out} = 7.00 mm, Φ_{in} = 3.04 mm) to prepare the tested specimens. The simulated RL was calculated from measured parameters (under coaxial wire analysis) based on the transmission line theory.

The EMWA properties of Cd-MOFs-500 are analyzed by determining the materials' dielectric and magnetic properties, as their functional relationship can be expressed by the following equations, according to the literature:

$$\mathrm{RL}(dB) = 20\log\left|\frac{Z_{in}-1}{Z_{in}+1}\right| \quad (1)$$

where Z_{in} is the normalized input impedance in free space and at the material interface and can be calculated by the following equation:

$$Z_{in} = \sqrt{\frac{\mu_r}{\varepsilon_r}} \tanh\left[j\left(\frac{2\pi}{c}\right)\sqrt{\mu_r \varepsilon_r} f d\right] \quad (2)$$

where f is the frequency of the electromagnetic wave, d is the thickness of the absorber, c is the velocity of light, μr (μr=μ′-μ″) and εr (εr=ε′-ε″) are the relative complex permeability and permittivity, respectively, and Zin is the input impedance of the absorber. The RL values for various sample thicknesses of Cd-MOFs-500 can be calculated according to equations 1 and 2.

X-ray crystallography

Optical microscope was used to select the appropriate size single crystal of MOF 2 before X-ray crystallographic data. An CCD detector with graphite-monochromatic Mo-Kα radiation (λ = 0.71073 Å) at 100 K (for MOF 2) by under the φ-ω scan mode was used for X-ray crystallographic data collecting on Bruker Smart Apex diffractometer. The date reduction was carried out with SAINT software and corrected for Lorentz and polarization effects. The SADABS program was used to perform a semi-empirical absorption correction on the diffraction intensity data, and an observable point of I>2σ(I) was selected for structural analysis and correction. the SHELXS program was used to determine the single crystal structure, and some non-hydrogen atoms were determined by subsequent differential Fourier synthesis. The coordinates and anisotropic thermal parameters for non-hydrogen atoms are corrected by the full-matrix least-squares method using the SHELXL-97 program. The scattering from the highly disordered lattice guest molecules were removed using the SQUEEZE procedure implemented in the PLATON package. Crystallographic data for MOF 2 are given in Table S1. Selected bond lengths and angles are listed in Table S 2.

Table S 1 Summary of crystal data and structure refinement parameters for MOFs [a]

MOFs	MOF **2**
Empirical formula	$C_4H_2CdN_2O_2$
Formula weight	222.48
Crystal system	Monoclinic
Space group	*C*2/*c*
a (Å)	12.2758 (5)
b (Å)	10.2771 (4)
c (Å)	7.5324 (3)
α (°)	90

β (°)	104.454 (1)
γ (°)	90
V (Å^3)	920.21 (6)
Z	8
D_{calcd}(Mg m^{-3})	3.212
μ (mm^{-1})	4.64
Reflections collected	4920
Data/parameters	911/844
F(000)	832
T (K)	100
R_{int}	0.031
Final R indices	R_1 = 0.0176
[I>2sigma(I)]	wR_2 = 0.0362
R indices (all data)	R_1 = 0.0153
	wR_2 = 0.0371
Gof	1.11

$^aR_1 = \Sigma\|F_o| - |F_c\|/\Sigma|F_o|$, $_wR_2 = [\Sigma_w(F_o^2 - F_c^2)^2]/[\Sigma_w(F_o^2)^2]^{1/2}$

Table S2. Selected bond lengths and angles for MOF **2**

	Length (Å) or Angle (°)		Length (Å) or Angle (°)
Cd1—O1^{i}	2.394 (2)	N1—Cd1—O1^{i}	94.91 (8)
Cd1—O1^{ii}	2.2688 (19)	N1—Cd1—O1^{ii}	84.75 (8)
Cd1—O2^{iii}	2.307 (2)	N1—Cd1—O2^{iii}	102.91 (8)
Cd1—N1	2.257 (2)	N2^{iv}—Cd1—O1^{i}	87.79 (7)
Cd1—N2^{iv}	2.251 (2)	N2^{iv}—Cd1—O1^{ii}	148.30 (8)
O1^{ii}—Cd1—O1^{i}	74.05 (8)	N2^{iv}—Cd1—O2^{iii}	91.61 (8)
O1^{ii}—Cd1—O2^{iii}	96.35 (7)	N2^{iv}—Cd1—N1	123.25 (8)
O2^{iii}—Cd1—O1^{i}	158.98 (7)		

Structure description of MOF 2

MOF **2** crystallized in the monoclinic space and exhibited *C*2/*c* space group. Single-crystal X-ray diffraction analysis revealed that MOF **1** exhibited 3D framework based on mononuclear structure and the symmetric unit of MOF **2** consisted of one six coordinated central ion Cd, and one organic linker. The central Cd ions were coordinated by four oxygen atoms and two nitrogen atoms from different organic linkers forming a distorted octahedron. The lengths of Cd-O bonds were range from 2.2688 (19) to 2.394 (2) Å, the lengths of Cd-N were 2.257 (2), 2.251 (2) Å, respectively. All MH ligands adopted one coordination mode μ_4-η^1-η^1-η^1-η^1 in MOF **2**. That meant each MH ligand coordinated to four central ions through two monodentate coordination carbonyl oxygen atoms and two nitrogen atoms, forming a dual-core [CdO_4N_2] secondary building unites (SBUs). Adjacent SBUs were interlinked by μ_4-MH forming a 3D open supramolecular architectures. Topologically, the framework of MOF **2** could be rationalized to a fee topology in which the inorganic metal ions and the organic linkers acted as 5-connected nodes.

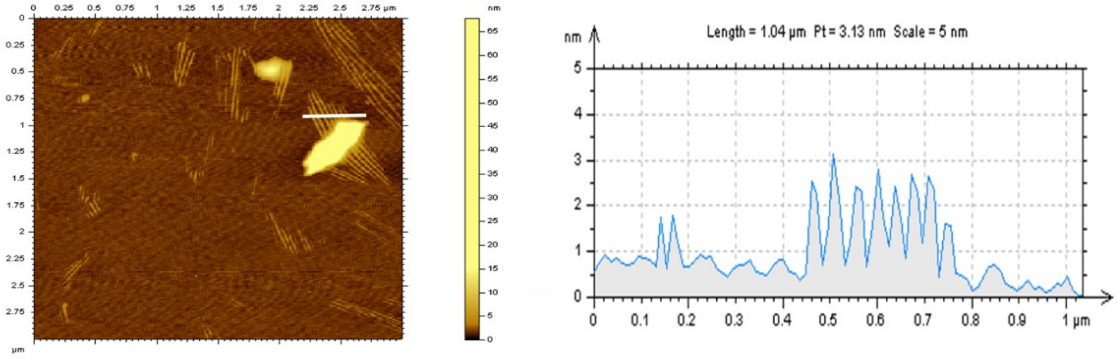

Fig. S1 AFM image of the nanobelts

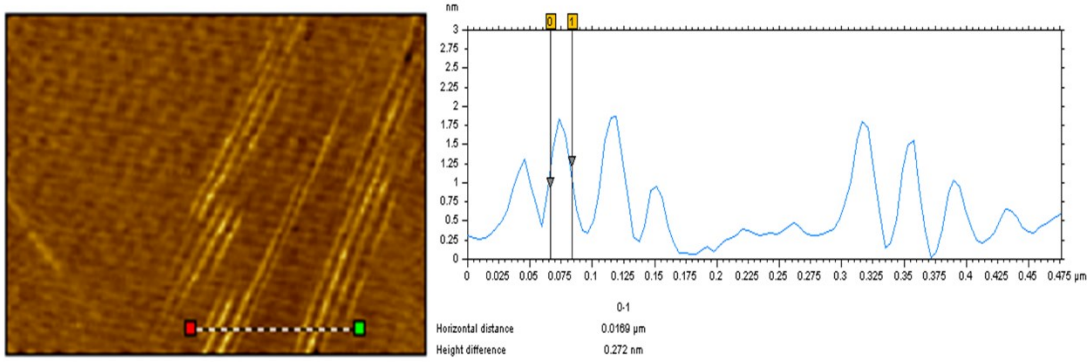

Fig.S2 the AFM image of the nanobelts

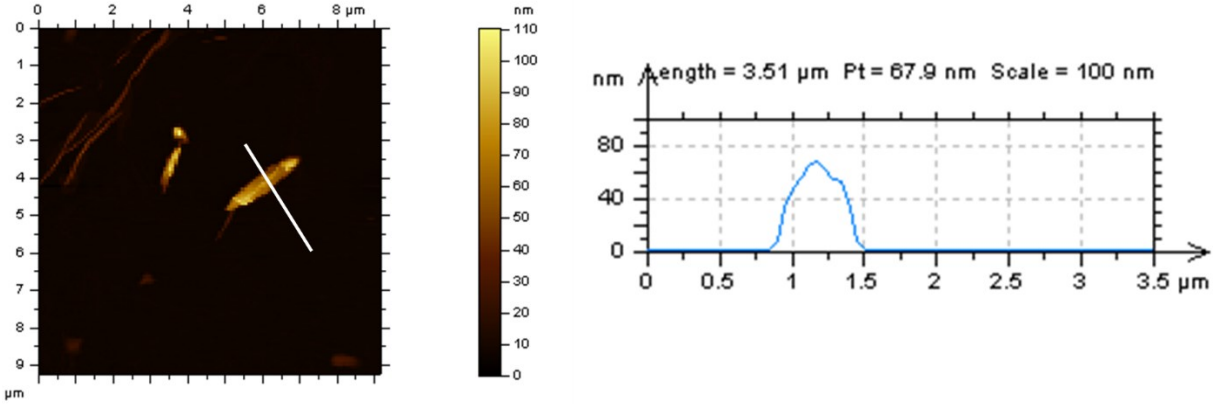

Fig. S3 the AFM image of the petal

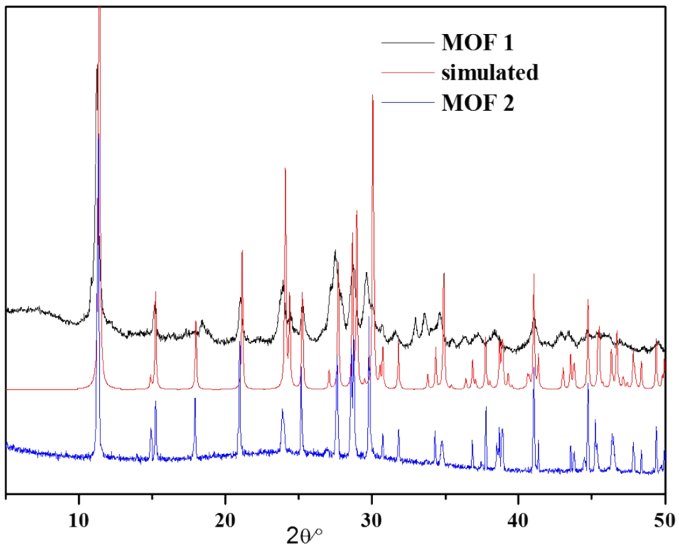

Fig. S4 Powder X-ray diffraction studies on MOFs **1-2**

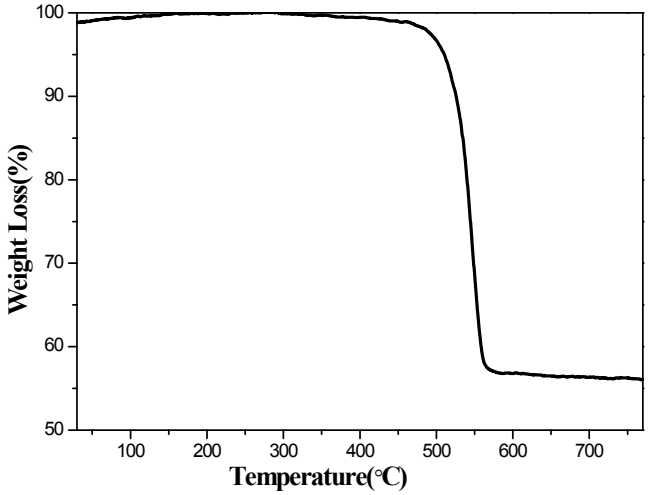

Fig. S5 TGA curve of the as-synthesized MOF **1**.

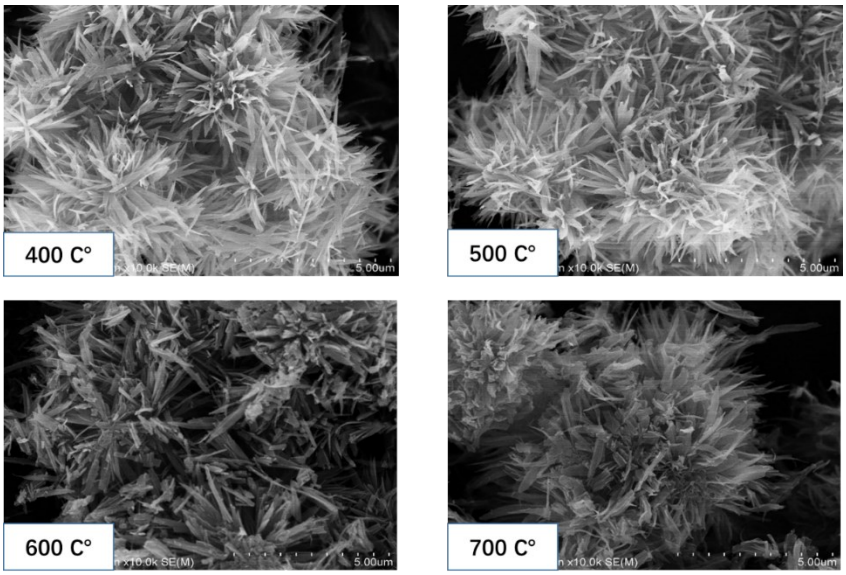

Fig. S6 SEM pictures of MOF **1** after pyrolyzation

The MOF kept generally stable under 400 and 500 °C. Beyond 500 °C, the morphology flower started to collapse apparently. As the Fig.S6 showed, when the pyrolysis temperature up to 600 and 700 °C, the morphology flower collapsed thoroughly indicating the framework of MOF **1** had collapsed violently.

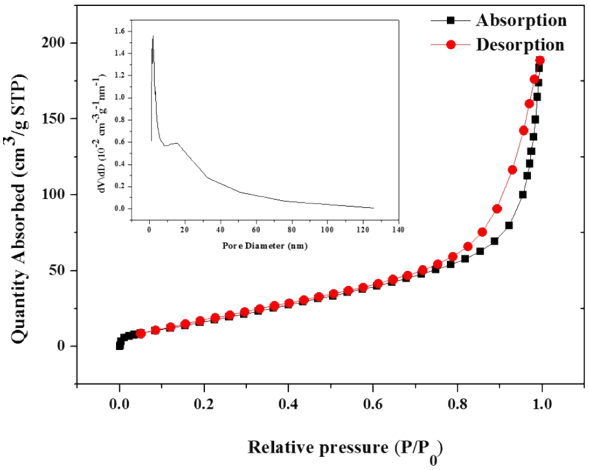

Fig. S7 N_2 adsorption-desorption isotherms of MOF **1**.

Table S3 The pore property of MOF 1

BET surface area	**68.33 $m^2 \cdot g^{-1}$**
Pore volume	**0.277 $cm^3 \cdot g$**
Adsorption average pore diameter	**15.0739 nm**
Median pore width	**1.1983 nm**

The pore property of MOF 1 is investigated by nitrogen adsorption-desorption

analysis. As shown in the above table, MOF 1 have the hierarchical pore structure. The BET surface area of 68.33 m2 ·g-1, the Pore volume of 0.277 cm3·g, the adsorption average pore diameter of 15.0739 nm and the median pore width of 1.1983 nm can be observed.

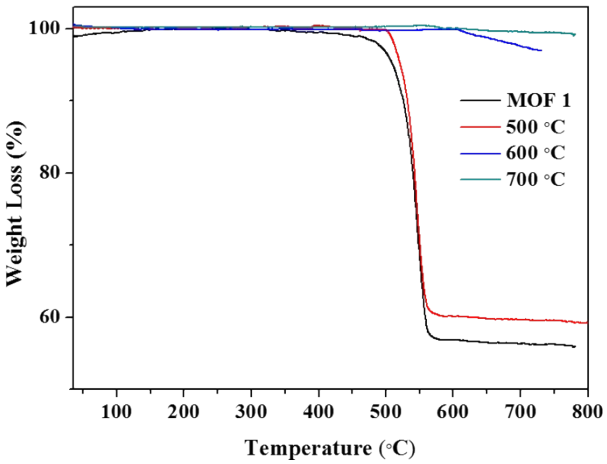

Fig S8 The TGA curves of MOF 1 and derived carbon materials

The TGA curves of the carbon materials demonstrate that MOF 1 is almost completely pyrolyzed at 600 ℃.

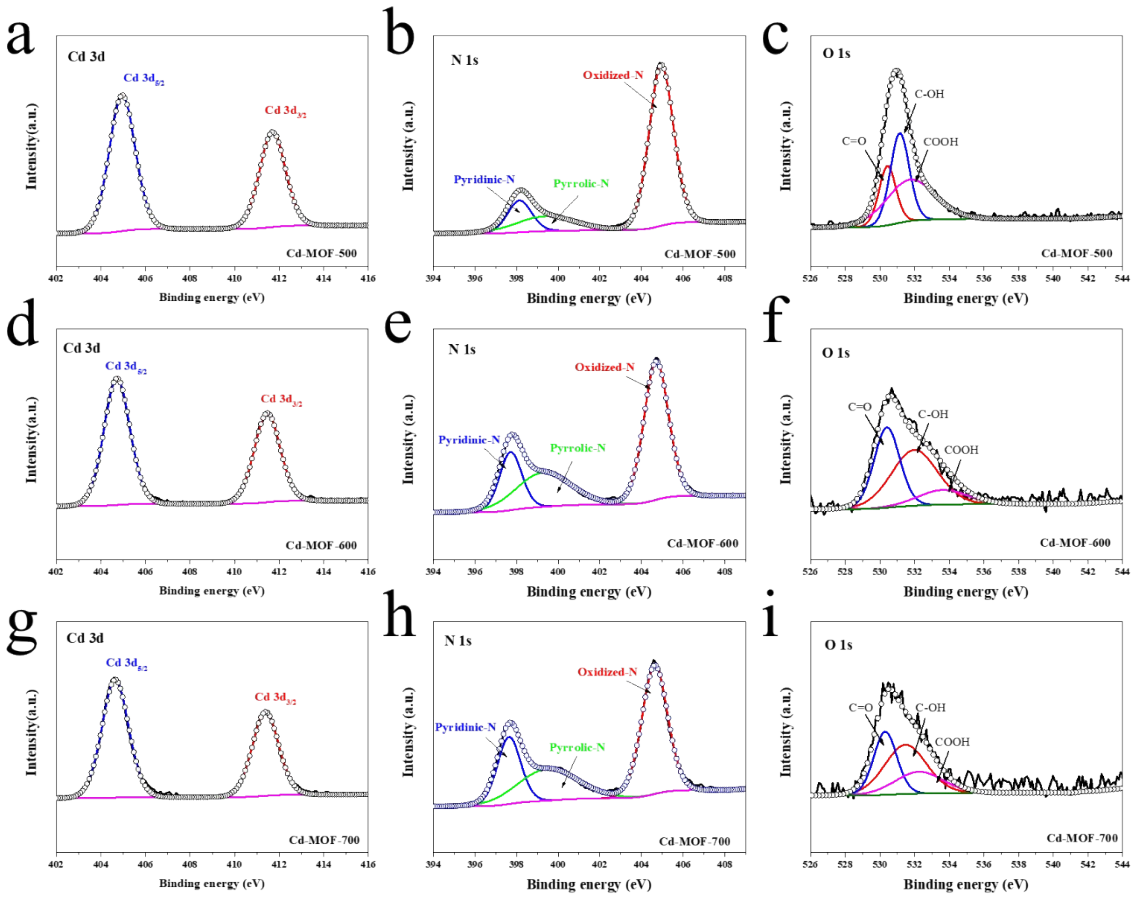

Fig. S9 XPS survey scan of Cd-MOFs; (a-c) Cd 3d, N 1s, and O 1s of Cd-MOF-500; (d-f) Cd 3d,

N 1s, and O 1s of Cd-MOF-600; (g-i) Cd 3d, N 1s, and O 1s of Cd-MOF-700.

The chemical state of elements was further investigated by analyzing the high-resolution Cd 3d, N 1s, and O 1s. The high resolution XPS spectrum of Cd 3d depicted in Fig.3 gives the binding energies of Cd $3d_{5/2}$ (404.7eV) and Cd $3d_{3/2}$ (411.5eV), indicating that the Cd element in the composite is Cd^{2+}. The surface redox reaction introduced by Cd^{2+} contributed part of the pseudocapacitance. The content of nitrogen in the Cd-MOFs is quite high, and the high-resolution N 1s spectrum was fitted with three individual peaks centered at 397.7 eV, 399.3 eV, 404.8 eV; these peaks are ascribed to pyridinic-N, pyrrolic-N, and oxidized-N. The O1s peak is segmented into three peaks situated at approximately 530.3 eV, 531.6 eV, and 533.2 eV, corresponding to C=O groups or quinone, C-OH groups or phenol, and COOH carboxyl groups, respectively.

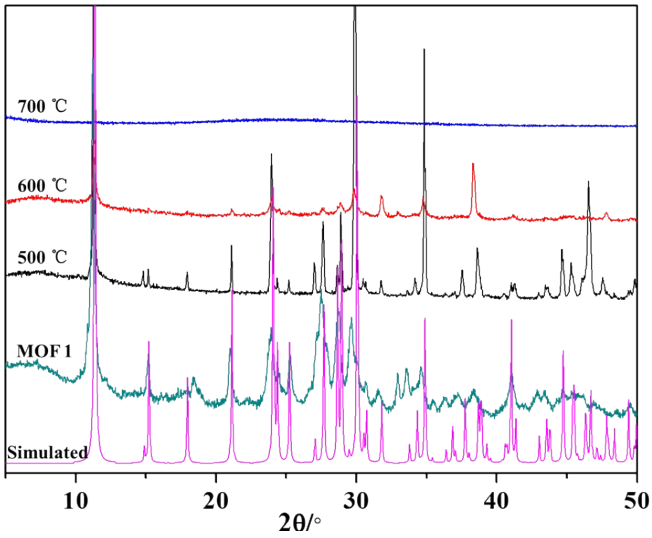

Fig. S10 temperature-dependent PXRD profiles of MOF **1** crystals under N2 protection

The temperature-dependent collapse of the framework was investigated by PXRD patterns. The intensity of the diffraction peaks of MOF 1 crystals gradually decreased with the temperature increasing, and finally disappeared at 700 ℃. The collapse of the structure suggested that the temperature of 700 ℃ was sufficient to convert MOF 1 into amorphous carbons.

The R_{ct} and R_s of Cd-MOFs-500 are less than that of Cd-MOFs-600 and Cd-MOFs-700. The small equivalent serial resistance and low charge transfer resistance give rise to the Cd-MOFs-500 excellent capacitive performance.

Table S4 Parameter of equivalent circuit elements

Samples	R_s (Ω)	R_{ct} (Ω)
Cd-MOFs-500	0.492	0.095
Cd-MOFs-600	0.502	0.174
Cd-MOFs-700	0.569	0.194

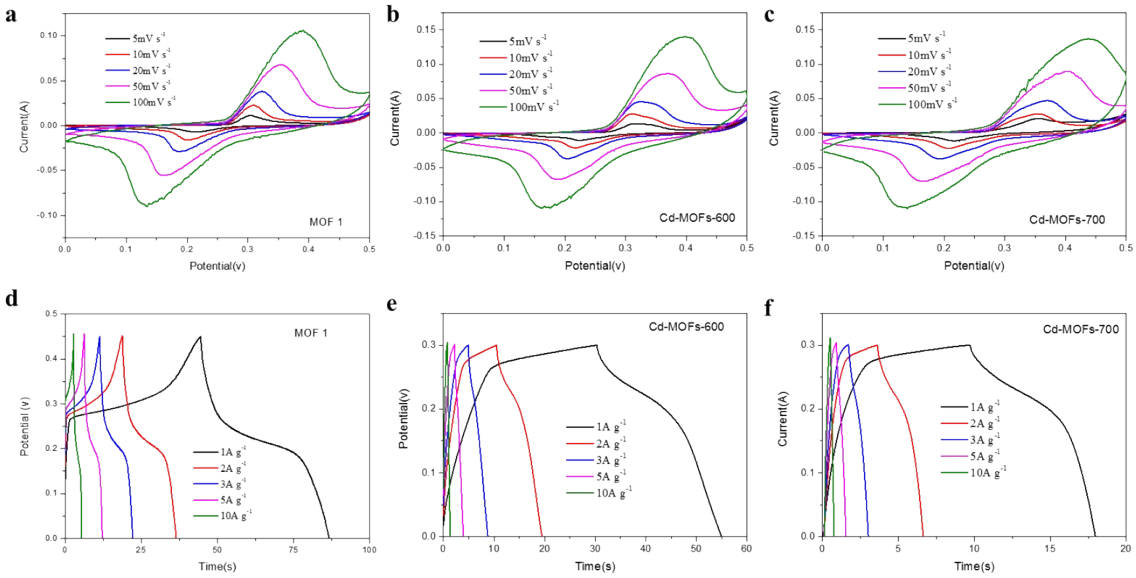

Fig. S11 The electrochemical parameters of MOF 1 and MOF 1 derived carbon materials.

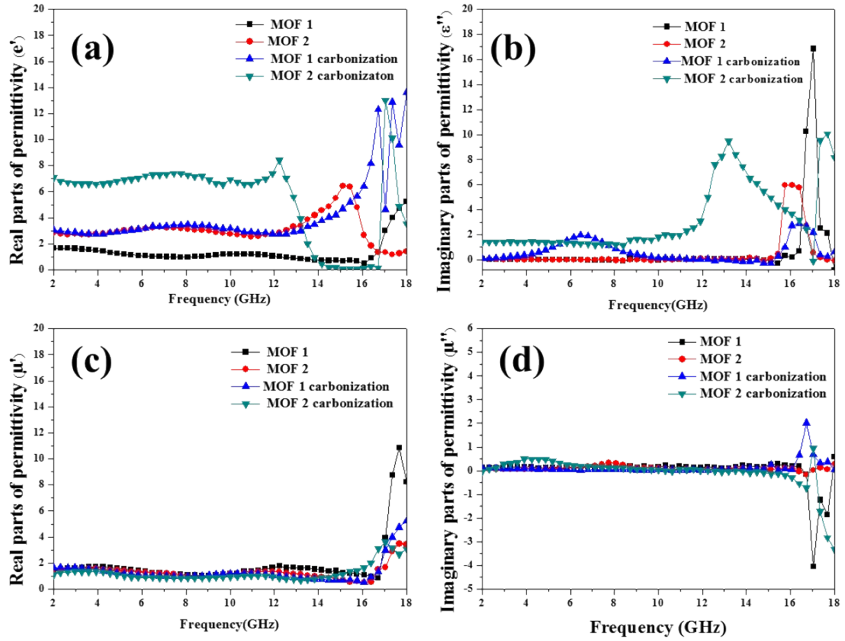

Fig S12 The relative permittivity (ε′, ε″) (a, b) and relative permeability (μ′, μ″) (c, d) of MOF

1-2.

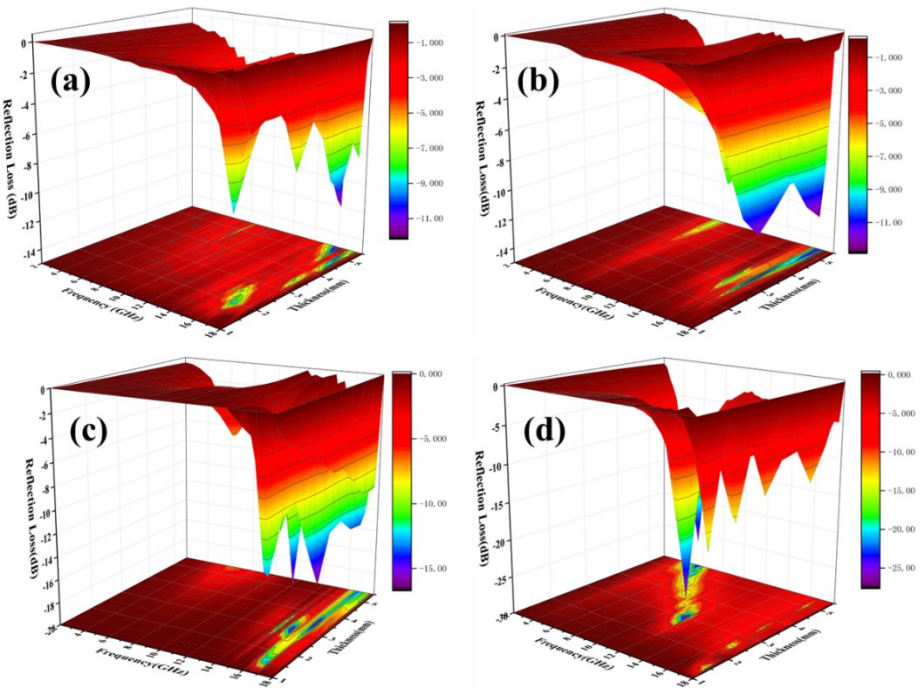

Fig. S13 The RL values of MOF **1-2[**(a): for MOF **2**，(b): for MOF **1**，(c): for MOF **2** after pyrolysis at 500 °C under nitrogen environment，(d): for MOF **1** after pyrolysis at 500 °C under nitrogen environment].

Fig. S13 shows the correlation among RL values, frequency, and thickness can be visually reflected through a three-dimensional (3D) plot of MOF 1, MOF 2 and MOF 1 derived carbon materials, MOF 2 derived carbon materials. The EMWA performance of MOF 1 derived carbon materials is discussed in manuscript. Therefore, the rest three materials are further discussed here. MOF 1 and MOF 2 exhibit significantly difference of EMWA performance as Fig. S13 manifests. More specifically, MOF 1 and its derived materials have better effective EMWA properties than MOF 2 and its derived materials, which may be attributed to the unique morphology of the titled materials. As is shown in Fig. S13a&b, the raw MOFs (without any pyrolysis) have barely effective absorption bandwidth. The maximum reflection loss of -19.27 dB at the 15.76 GHz can be observed for MOF 2 at the thickness of 5.5 mm. As for MOF 1, -10.66 dB GHz can be obtained at under the thickness of 2.5 mm. After pyrolysis, MOF 2 derived carbon materials can research the maximum reflection loss of -16.54 dB at the 17.12 GHz and show more effective EMWA absorption in the wider band comparing with MOF 2.

As Fig. S12 manifests, the conductivities of both MOF 1 MOF 2 derived carbon materials are significantly enhanced after pyrolysis, which may lead to the better EMWA performances.

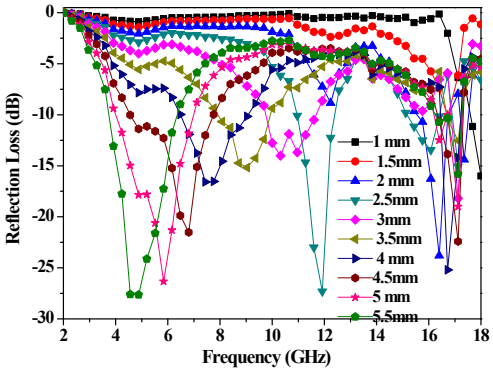

Fig S14 The RL values (a) of Cd-MOFs-500

Table S5 Typical properties and applications of Cd based metal-organic frameworks in near two years

Compound	Application	Achieve Value or year of report	Reference
Cd-MOF	luminescent sensor	0.1 μM for nitrobenzene and 3 nM for parathion-methyl	[1]
$Cd(NIPA)(CH_3CH_2OH)_3$	supercapacitor	367 F g^{-1} at 1 A/g	[2]
Complex 1	fluorescent probe	detection limits is200 nM	[3]
MoS2@Cd-MOF	Photocatalytic Hydrogen Evolution	5587 $\mu mol \cdot h^{-1} \cdot g^{-1}$	[4]
$Cd3(BTC)_2(4\text{-}bpdb)_2$	adsorbent of organic dyes and precursor of CdO nanoparticles	2020	[5]

From the table of "typical properties and applications of Cd based metal-organic frameworks in near two years", one can found that the application of Cd based MOF materials are focused on the sensor, catalyzer, adsorbent and supercapacitor materials. Compared with $Cd(NIPA)(CH_3CH_2OH)_3$, even they have a better electrochemical performance, the much more complicated preparation process also is the significant shortcoming. It is worth noting that there are not any Cd based MOFs with the unique morphology reported. And as far as we know, it is the first time to report the EMWA of Cd based MOFs in our manuscript.